BUILD SIMUL (2022) 15: 859–870
https://doi.org/10.1007/s12273-021-0836-1

Quantitative distribution of human exhaled particles in a ventilation room

Zhijian Liu[1], Hangyao Zhu[1], Yangfan Song[1] (✉), Guoqing Cao[2]

1. Department of Power Engineering, North China Electric Power University, Baoding 071003, China
2. Institute of Building Environment and Energy, China Academy of Building Research, Beijing 100013, China

Abstract

Respiratory viruses can be attached to human exhaled particles and spread from person to person through respiratory activities. The purpose of this study is to obtain the quantitative description formula of human exhaled particles in the ventilated room through amount number of numerical simulation calculations and regression statistical analysis of the simulated data. In this study, a combination of numerical simulation and laboratory experiments was used, and the results were tallied preferably. Bacillus subtilis was released as a release source to investigate the migration and distribution of bioaerosol. The results show that under the condition of high air supply velocity, due to the disturbance of human respiration and airflow, the diffusion velocity of exhaled particles was faster and the diffusion range is larger than that of low air supply velocity within the same time frame. No matter where the location of the manikin was in the room, the exhaled particles would spread to the whole room in at least 900 s. The method used in this study could be used to predict the distribution of human exhaled particles concentration in different indoor spaces, such as public transport and hospitals. These findings could provide valuable reference for the location of indoor air purifiers, which plays a guiding role in the construction of a healthy indoor environment.

Keywords

droplet aerosols;
particulate concentrations;
bioaerosol release experiment;
CFD predictions

Article History

Received: 17 May 2021
Revised: 13 August 2021
Accepted: 19 August 2021

1 Introduction

Recently, the global epidemic of the COVID-19 virus has posed a massive threat to human life and health (Wu et al. 2020). There have been similar outbreaks of large-scale respiratory infections in history, such as the MERS virus in 2015, H1N1 virus in 2009, and SARS virus in 2003. In 2015, active influenza A virus was detected in aerosol particles released from cough of influenza patients (Lindsley et al. 2015). In 2019, viable SARS-CoV-2 virus can be detected in aerosols generated by COVID-19 patients in a hospital room (Ge et al. 2020; Lednicky et al. 2020; Yao et al. 2020). The above studies and a large amount of other evidence have shown that expiratory particles can serve as a source for virus transmission. Indoor aerosols, the core and carriers of virus and bacteria transmission have attracted more and more attention.

Most people spend nearly 85%–90% of their lifetime indoors, so indoor air quality is tightly related to human health (Chen et al. 2020). Considering the spatial distribution of indoor particles is thus helpful in providing a basis for reducing indoor particle concentration and improving indoor air quality, which is of great significance for the accurate design of a healthy indoor environment. To date, the distribution and propagation of aerosols and other apparent properties have been studied in many indoor places, such as public hospitals (Chow and Wang 2012; Sadrizadeh et al. 2014; Wang et al. 2018), workplaces (Kalogerakis et al. 2005; He et al. 2011; Zhang et al. 2017), houses (Lis and Pastuszka 1997; Jo and Seo 2005; Guo et al. 2020), and public restrooms (Lee et al. 2012; Kim et al. 2014; Sassi et al. 2018). At the same time, more in-depth and rigorous researches on aerosols have been carried out. Short-distance droplet transmission is dominant among various recognized transmission routes of respiratory infectious diseases (Xie et al. 2007). Pathogen-laden droplets are released from the infector by breathing, speaking, coughing,

E-mail: yfsong@ncepu.edu.cn

sneezing, and other different respiratory activities (Morawska et al. 2009; Bourouiba et al. 2014; Kang et al. 2015). Liu et al. (2017) studied gaseous pollutant transmission characteristics under different ventilation strategies by computational fluid dynamics (CFD) method in a typical chemical laboratory and found out three dominant factors, including the location of the pollution source and air supply conditions. Zhang and Chen (2009) used the Lagrange method to accurately predict the exposure risk of the particulate matter in buildings to the residents. Through numerical simulation, Chen and Zhao (2010) discussed the effects of evaporation, ventilation pattern, ventilation volume, initial expiratory velocity, temperature, relative humidity and initial particle size on the diffusion of human exhaled droplets aerosols.

The indoor CFD method can predict various flow fields and particle diffusions by simulation, providing valuable information for solving indoor air quality problems (Srebric et al. 2008) and has been widely used in various prediction studies. To the Eulerian method, particles are treated as a continuum and solve the conservation equations for the particle phase. As for the Lagrangian method, it emphasizes the individual behavior of each particle and determines particle trajectories based on the motion equation. Compared with full-scale experiments, the cost of time using CFD technology is lower. However, although obtaining the actual measured data is more time-consuming and less convenient than CFD technology, experiments also have a certain value by providing the real dispersion mechanism of fluid and particles (Jurelionis et al. 2015).

Most of the existing studies are based on CFD technology to describe the aerosol distribution qualitatively, but there are few studies on quantitative description of human exhaled bioaerosol indoors. The particle mass concentration at any point under various conditions can be obtained by numerical simulation in three-dimensional space. However, in practice, it is impossible to change the boundary conditions at any time and carry out long-term simulation calculations to get the particle mass concentration. Therefore, the purpose of this study was to determine the quantitative description formula of human exhaled particles in a ventilation room through amount number of numerical simulation calculations and regression statistical analysis of simulated data. Additionally, it also considers whether there is a multiple superposition of the quantitative description formula when there are many people under the same condition in the room. Fourteen single-person cases including different air supply velocities (0.16 , 0.28, and 0.33 m/s), air supply temperatures (10, 20, and 30 °C), and the locations of manikin were set in the CFD numerical simulation. Simultaneously, six multi-person conditions were also set. What's more, the CFD models were validated by the test chamber and manikin experiments with the same size as the numerical model.

2 Simulation setup

2.1 Governing equations

The following three simulation methods are usually used for indoor airflow, the direct numerical simulation (DNS), the large eddy simulation (LES) and the Reynolds-averaged Navier-Stokes (RANS) methods. The DNS and LES methods require much computing resources and time. The RANS method consumes less computation time and has relatively high accuracy, so it is the most common and effective method for indoor airflow. In this study, the airflow pattern of the laboratory was assumed to be incompressible and turbulent with low speed. Therefore the RNG k-ε model belonging to the RANS was adopted in the present study, which has been proved to be suitable for simulating the complex indoor airflow field (Srebric et al. 2008; Romano et al. 2015; Wang et al. 2021). The general form of the governing equation of the RNG k-ε model is as follows:

$$\frac{\partial(\rho\phi)}{\partial t}+\nabla\cdot\left(\rho\phi\vec{V}\right)=\nabla\cdot\left(\Gamma_{\phi}\nabla\phi\right)+S_{\phi} \tag{1}$$

where ρ is the density of the air; $\vec{V}$ is the velocity vector of the air, ϕ is a general variable, it can represent the velocity components (u, v, w), thermodynamic temperature T and other variables; Γ_{ϕ} is the effective diffusion coefficient of ϕ; S_{ϕ} is the source term.

The Lagrangian discrete tracking model was adopted in this study to track the trajectories of spherical particles in the continuous fluid. Based on the analysis of previous studies (Zhao et al. 2008; Yan et al. 2017), the driving forces of small-sized particles such as pressure gradient force, virtual mass force and Basset history are lower in magnitude compared with other forces therefore ignored in this study. The effect of the Brownian force is ignored since it has a more negligible effect on the particles with a size larger than 0.5 μm (Chang and Hu 2008). Thus, only the drag force $\vec{F}_{\mathrm{D}}$, the gravity $\vec{F}_{\mathrm{G}}$, the Saffman's lift force $\vec{F}_{\mathrm{S}}$, and thermophoretic force $\vec{F}_{\mathrm{T}}$, were considered in this study. The motion of the particles can be described as follows:

$$m_{\mathrm{p}}\frac{\mathrm{d}u_{\mathrm{p}}}{\mathrm{d}t}=\vec{F}_{\mathrm{D}}+\vec{F}_{\mathrm{G}}+\vec{F}_{\mathrm{S}}+\vec{F}_{\mathrm{T}} \tag{2}$$

$$F_{\mathrm{D}}=\frac{18u_{\mathrm{a}}}{\rho_{\mathrm{p}}d_{\mathrm{p}}^{2}C_{\mathrm{c}}}\left(u-u_{\mathrm{p}}\right) \tag{3}$$

$$F_{\mathrm{G}}=\frac{\pi}{6}d_{\mathrm{p}}^{3}\rho_{\mathrm{p}}g \tag{4}$$

$$F_{\mathrm{S}}=\frac{1.62\mu d_{\mathrm{p}}^{2}\left(\mathrm{d}u/\mathrm{d}y\right)}{\sqrt{\nu\left|\mathrm{d}u/\mathrm{d}y\right|}}\left(u_{\mathrm{a}}-u_{\mathrm{px}}\right) \tag{5}$$

$$F_T = 3\pi\mu d_p B|\Delta T| \quad (6)$$

where u_a represents the fluid viscosity, ρ_p is the particle density, d_p refers to the particle size and C_c is the Cunningham correction factor, u is the air velocity, and u_p is the particle velocity, g refers to the gravitational acceleration, du/dy is the air velocity gradient perpendicular to the wall surface, u_{px} is the particle axial velocity, B is the thermophoretic force coefficient.

The Cunningham correction factor is approximated as (Lee and Liu 1982):

$$C_c = 1 + 2.493\frac{\lambda}{d_p} + 0.84\frac{\lambda}{d_p}\exp\left(-0.435\frac{d_p}{\lambda}\right) \approx 1 + \frac{3.34\lambda}{d_p} \quad (7)$$

where λ is the fluid molecule mean free path.

The thermophoretic force coefficient is defined as (Dong et al. 2017):

$$B = \frac{2\mu C_s (K + C_t K_n)}{\rho(1 + 3C_m K_n)(1 + 2K + 2C_t K_n)}\frac{1}{T} \quad (8)$$

where C_t, C_m and C_s represent the thermal exchange coefficient and the thermal slip coefficient respectively, K denotes the ratio of the thermal conductivity of the particles to the fluid and K_n is the Knudsen number.

Furthermore, the discrete random walk model (DRW) is also used to obtain the diffusion of particles with turbulence pulsation. The DRW model assumed that particles interact with a series of eddy for an interaction time interval, but not with each other (Elghobashi 1991). Each eddy has a characteristic time and a characteristic scale. When the characteristic time of the eddy ends or the particle passes through the eddy, the particle will interact with the next turbulence eddy.

The evaporation model has not been turned on in order to simplify the calculation, thus, the effect of volatile content on droplet aerosols surface vapor molar concentration was not taken into account.

2.2 Geometry and grid

Figure 1 shows the three-dimensional computational geometry of a full-scale room, with a size of 5.4 m × 6.6 m × 3 m ($X \times Y \times Z$). There are four inlets on the ceiling and five outlets on each side of the room. The female manikin body model with the shape and size of human bodies is applied to carry out the numerical simulation. The height of female manikin is 1.67 m and the total surface area is 1.49 m^2 approximately. Suppose the direction of the initial respiratory airflow velocity is horizontal.

As illustrated in Figure 1, three lines were used to divide the length and width of the room into four parts. Thus, there were nine intersections, namely nine kinds of personnel positions in the experiment. Considering the symmetry, four of them were selected for the experiment under single-person conditions. More details about the locations of manikin were shown in Table 1.

Unstructured grids are used around the manikin due to the complex geometry. The mesh around the face of the female manikin is refined to come up to the high-precision local grid system required by high concentration, velocity and temperature gradient in the respiratory region. Besides, the grid size of the inlet, outlet and manikin surface is minished. Before the study, three grid sizes of 1 cm, 2 cm, and 5 cm are used to verify the grid independence, and three sets of grids with the numbers of 1,273,397, 1,666,448, and 3,536,152 were numerically simulated. In this study, the air supply velocity at the air supply outlet and the position of the human body are the main influencing factors of airflow. Therefore, a

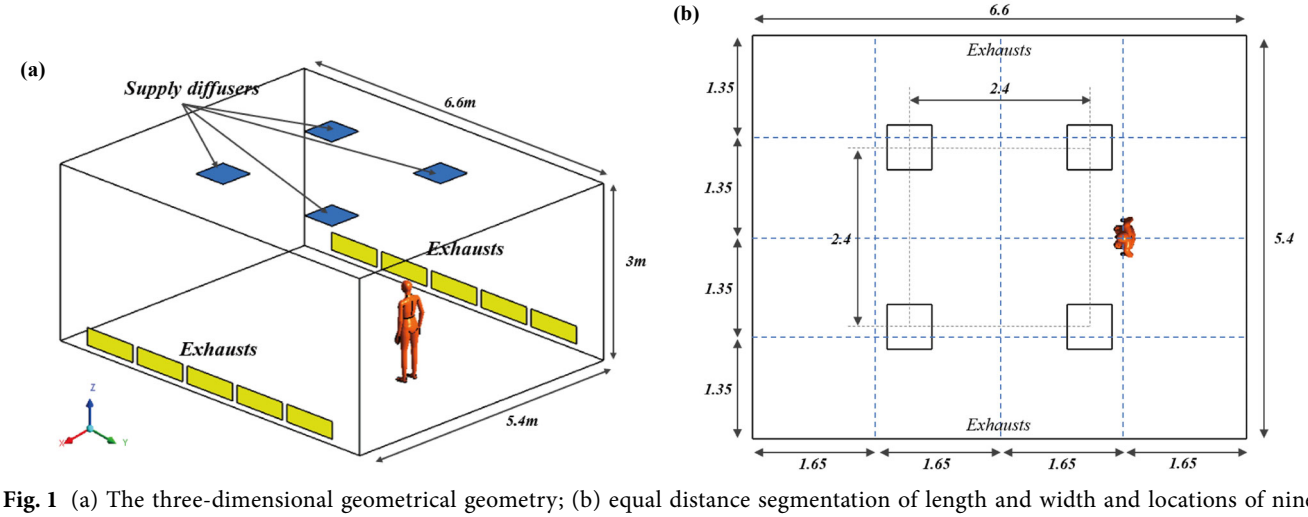

Fig. 1 (a) The three-dimensional geometrical geometry; (b) equal distance segmentation of length and width and locations of nine intersections (unit: m)

Table 1 Simulation cases

Case No.	Supply air temperature (°C)	Supply air velocity (m/s)	Locations of manikin
Case1	20	0.16	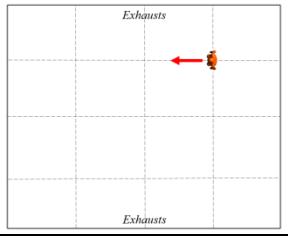
Case2	20	0.28	
Case3	20	0.33	
Case4	20	0.16	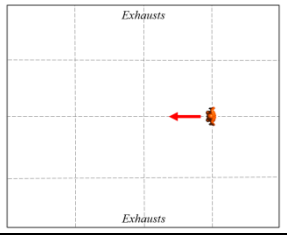
Case5	20	0.28	
Case6	20	0.33	
Case7	20	0.16	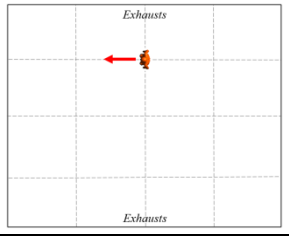
Case8	20	0.28	
Case9	20	0.33	
Case10	20	0.16	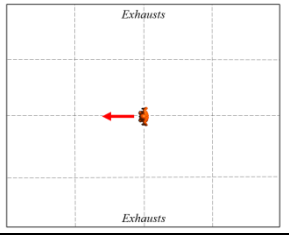
Case11	20	0.28	
Case12	20	0.33	
Case13	20	0.16	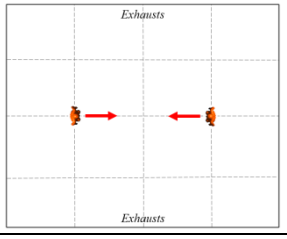
Case14	20	0.28	
Case15	20	0.33	
Case16	20	0.16	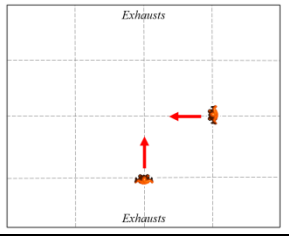
Case17	20	0.28	
Case18	20	0.33	
Case19	10	0.33	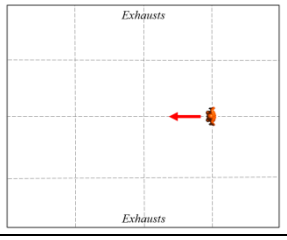
Case20	30	0.33	

horizontal straight line close to the human body and located under the two air supply outlets are selected for the grid independence test (He et al. 2011). The connection point is (4.05, 0, 1)(4.05, 6.6, 1). The results are shown in Figure 2, which shows little effect on the velocity field caused by the impact of the increase of the grid density. As a consequence, we believe that 1,273,397 grids are sufficient for the case study.

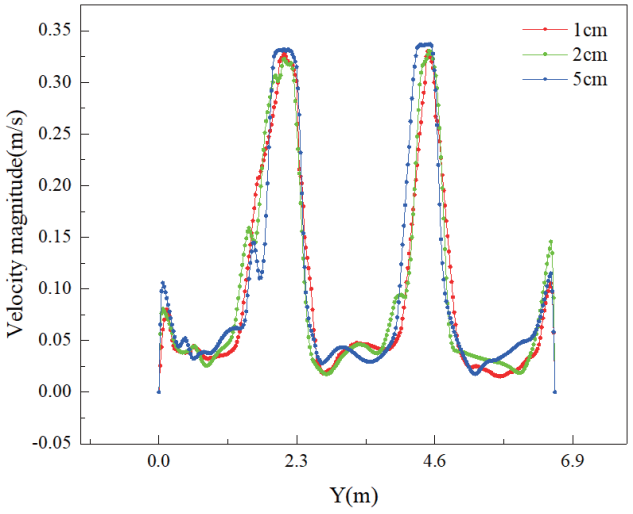

Fig. 2 The grid independence analysis

2.3 Boundary conditions and simulation cases

CFD simulations were carried out by applying ANSYS Fluent 17.0. In the simulation procedure, the turbulent flow field was calculated first, then the discrete particles were added and finally the coupled confluence was solved. When the particle arrived at the outlets of the ventilation, the trajectory calculation of the particle is terminated and the particle was considered to have left the room. In other words, the outlets were set as the escape boundary condition. When the particles were trapped on the wall, the wall was set under trapped boundary conditions because the particles could not accumulate enough bounce energy to overcome their adhesion (Hinds 1999). The emission type of particles adopts the discrete phase model (DPM) model point emission type in Fluent 17.0. To ensure the consistency between the numerical simulation and the experiment, the injection point used in the simulation was the same location as that used in the experiment. The initial velocity of particle release is 1.5 m/s, with the direction towards the direction of the human body. The particles were simulated as spherical particles with a density of 1000 kg/m^3 and a diameter of 2.5 μm, which was determined by the mass median diameter of the particles ejected from the aerosol generator. The manikin was set as a heat source intensity of 40 W/m^2 without considering the radiation or latent heat (Zukowska et al. 2012). The respiratory boundary condition at the mouth was set at a constant speed of 1.5 m/s, lasting 900 s. All air inlets were set as velocity inlets with a turbulent intensity of 5%. All exhausts were set as pressure outlet boundaries, with pressure at +25 Pa and a turbulent intensity of 5% (Chow and Wang 2012). The air is assumed to be incompressible and isothermal. The SIMPLE algorithm (Patankar and Spalding 1967) was adapted to couple the pressure and velocity fields. The Least Squares Cell-Based was used for the gradient discretization, and the staggered scheme named PRESTO! was applied for the pressure discretization. The Second Order Upwind is chosen to discretize the convection terms for the energy and momentum governing equations (Chow and Yang 2003; Chow et al. 2006). For converged solutions, the scaled velocity and continuity residuals reached 10^{-4}, and the energy residual reached 10^{-6}.

Four release rates (500, 1500, 3000, and 6000 CFU/s) have assumed before the simulation to verify the sensitivity of the particle number, and compared the simulated particle concentrations with the experimental results at the same sampling point by dimensionless concentration. Figure 3 shows the dimensionless standardized concentrations of the particles with four different release rates were basically consistent at the sampling point. To reduce the burden of computer and ensure the accuracy of simulation, the rate of 500 CFU/s was selected for the subsequent transient simulation.

This simulation first calculates the flow field under steady-state conditions. After convergence, particles were injected through the DPM model and converted to unsteady state conditions for calculation. The time step is 0.5 s, and the total calculation is 900 s, namely 15 min. Table 1 provides a summary of the simulation cases.

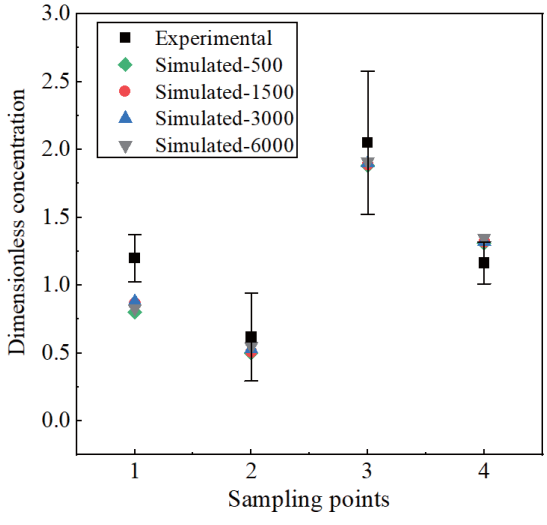

Fig. 3 Comparison of experimental and simulated values of dimensionless normalized concentrations

3 Experimental setup

The experiment was carried out in the State Key Laboratory of China Academy of Building Sciences. An environment chamber with the same simulated size was designed as a model space for aerosol distribution analysis. The floor, walls, and ceiling of the room are made of PVC material. The layout of the return air outlet in the ventilation room is shown in Figure 4. The size of a single air outlet is 0.54 m (L) × 0.54 m (W). The air supply velocity from the diffusers can be controlled by computer frequency conversion. The room is equipped with a single teardrop fluorescent lamp (28 W), surrounded by the air supply ceiling. The ventilation room has a total of 10 outlets, with five on each sidewall. In this experiment, an anemometer (TSI 8465) was used to measure indoor airflow velocity. The measuring range of the anemometer is between 0.01 m/s and 5m/s, with an accuracy of 0.01 m/s.

An aerosol generator was used to release bacteria-carrying particles (BCPs). The suspension of Bacillus subtilis was used in the bacteria generation experiment. This strain was easy to be cultivated and could grow on the general medium. After culture, orange-red bacterial colonies were formed, which was easy to identify and easy to eliminate other miscellany bacteria in the air that fell on the medium, as is shown in Figures 6(b) and (c).The aerosol generator was made by an air pump connected to a container equipped with a Laskin nozzle (φ = 12 mm). The release rate of live Bacillus subtilis solution in the container was about 10 L/min under the steady pressure of the pump, and the release direction was forward. The aerosol generator is placed at the breathing height of the human body.

Two kinds of aerosol samplers were used in this experiment, namely Anderson six-stage sampler and the Lighthouse Active100 sampler. The sampling flow rate and sampling time of the Anderson six-stage sampler are 28.3 L/min and 5 minutes, respectively. And the sampling flow of the Active100 sampler was 140 L, the sampling time was less than five minutes. The locations of the anemometers were shown in Figure 5, and the bioaerosol concentration sampling points in the ventilation room are shown in Figure 5 and Figure 6(a). This experiment carried out a total of four groups of conditions, and each group of condition carried out three repeated experiments. The concentration of the suspension of Bacillus subtilis was 1.415×10^7 CFU/mL, and the average consumption of each experiment was 4.67 mL. Therefore, the calculated bacteria-producing flow was 4.4×10^6 CFU/min. Before each experiment, the indoor air supply device would be opened for ventilation for 10 min to remove indoor bacteria and form a stable flow field. Then, the bioaerosol generator will be opened and the sampler would be opened for sampling after 10 min. After sampling for 5 min, the aerosol sampler and aerosol generator were turned off successively after the sampling, and the collected petri dishes were placed in an incubator at 37 °C for 48 h.

The concentration of culturable bioaerosol in the air was calculated by:

$$C(\mathrm{CFU/m^3}) = \frac{\sum_{i=1}^{6} P_{r_i} \times 1000}{T(\mathrm{min}) \times F(\mathrm{L/min})} \tag{9}$$

where C is the concentration of culturable microorganisms in the air, P_{r_i} is the number of colonies at the i level, T is the sampling time, and F is the sampling flow rate.

4 Results and discussion

4.1 Model validation

A comparison of the experimental data and the simulated airflow velocity values in the environment chamber are shown in Figure 7. The results show that the simulated values were agreed with the experimental data, which verified the airflow phase model.

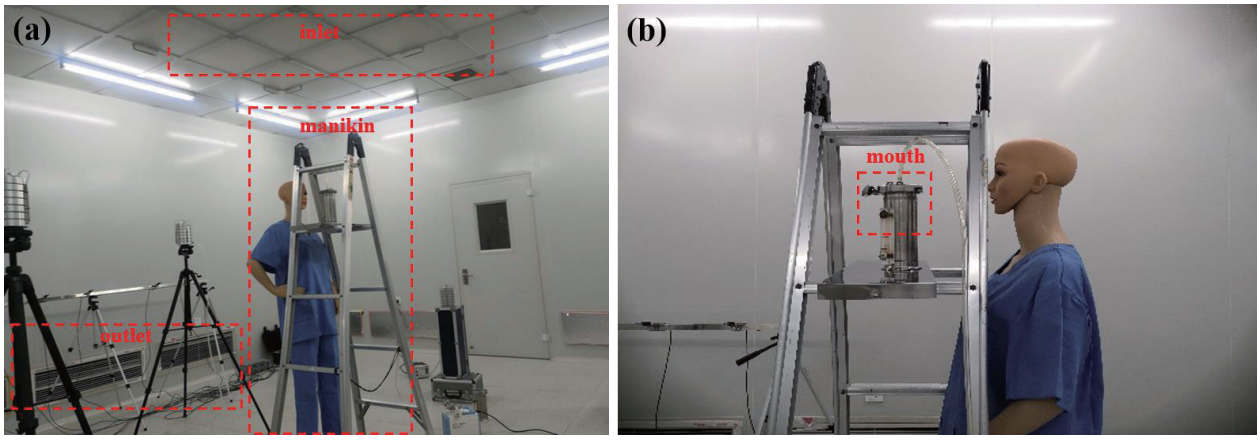

Fig. 4 (a) The configuration of the environment cabin; (b) the location of bioaerosol generator

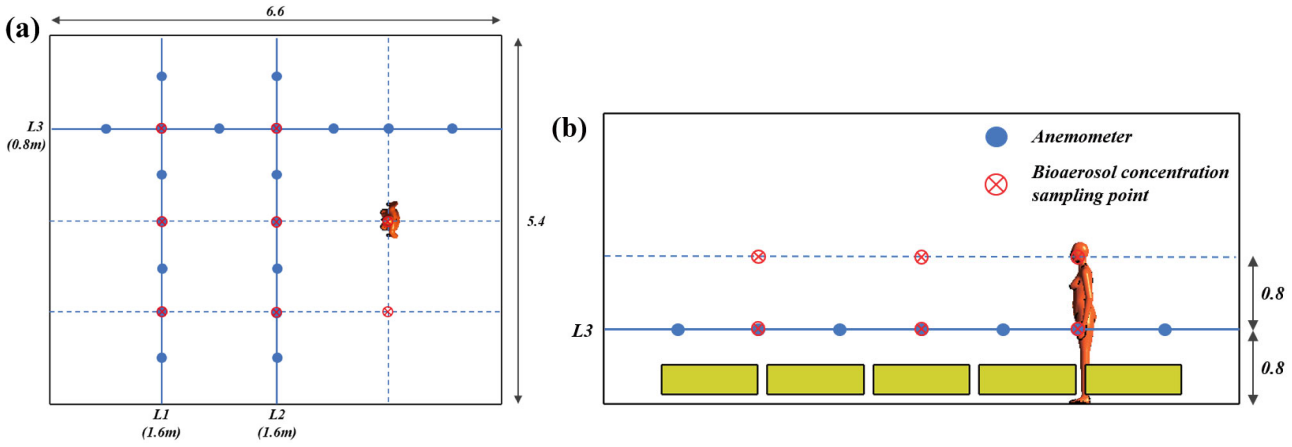

Fig. 5 The location of the anemometers, and bioaerosol concentration sampling points: (a) top view; (b) front view

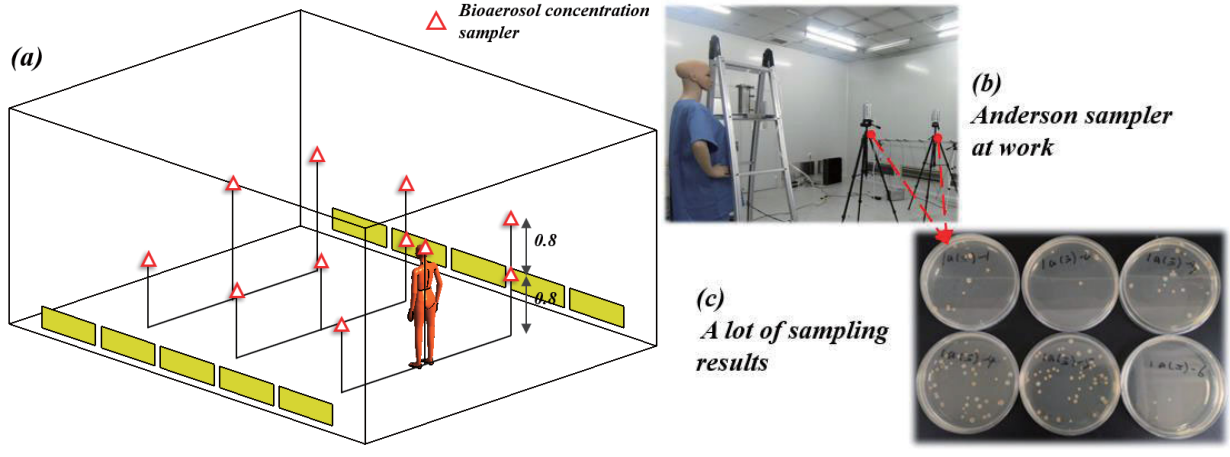

Fig. 6 Layout of the bioaerosol samplers

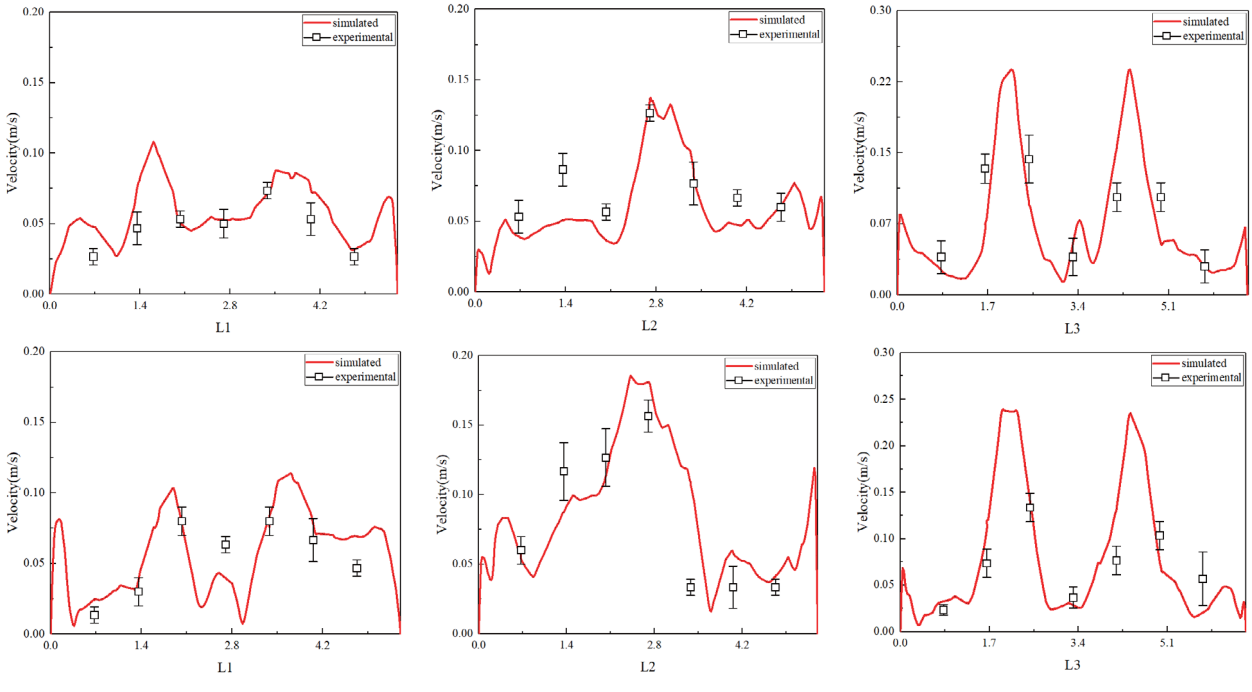

Fig. 7 Comparison of the experimental and simulated values of airflow velocity

In this section, the CFD model was verified by discussing and comparing experimental data and simulation values. It is not easy to directly compare experimental data with those simulation results. Therefore, the experimental and simulation results were compared by a dimensionless concentration. For the simulation, the particle concentrations at the same locations as the 4 test points were counted, and the particle concentration data at 5 min after each test point was averaged. Then the average particle concentration at the 4 test points was used as the denominator for dimensionless. It is defined as:

$$C(\%) = \frac{\overline{C}_x}{C_0} \tag{10}$$

where $\overline{C}_x$ is the average aerosol concentration at the measuring point x in the last 5 min; C_0 is the mean value of particle concentration at four measurement points. The dimensionless concentration after the calculation of the experiment and simulation results are shown in Table 2. The simulation values are agreed with the experimental data. For the four cases, at least two of the maximum dimensionless difference between the simulation and experimental results of the four measuring points in each group are less than 0.05. It means that the present numerical method could legitimately predict the aerosols distribution.

4.2 Particle distribution

Figure 8 shows the degree of particle dispersion at different times in case 6. Due to the high air supply velocity and the airflow disturbance, the aerosol exhaled by the human body eventually diffuses to the whole room. Same at 150 s, compared with case 6, the particles in case 13 diffuses more slowly due to the lower air velocity in Figure 9, and the diffusion range is smaller. At 900 s, the whole room is also filled with aerosol.

4.3 The correlation of particle distribution and variables

Based on the numerical simulation results in this study, the correlation between the average particle mass concentration on a horizontal section of the room at t = 900 s and the variables were numerically regressed:

$$\overline{C_z} = \left[1.76 \times \left(\frac{x}{W}\right)^{4.48} \times \left(\frac{y}{L}\right)^{-7.86} \times \left(\frac{z}{H}\right)^{1.07} \times \left(\frac{u_g}{u_i}\right)^{-3.12} \times \left(\frac{T_g}{T_i}\right)^{-3.12} + 860.44\right] \times 10^{-16} \tag{11}$$

where $\overline{C_z}$ is the average particle concentration on a horizontal section of the room; W, L, H represent the width, length, and height of the room, respectively; (x, y) represents the position of the person releasing the particles; z is the

Table 2 The dimensionless concentration of experiment and simulation results

	Point1	Point2	Point3	Point4
Case1	0.68	0.22	—	0.10
Simulation1	0.55	0.24	—	0.12
Case2	0.76	0.01	0.12	0.11
Simulation2	0.53	0.02	0.16	0.28
Case3	0.01	0.25	0.71	0.02
Simulation3	0.17	0.23	0.38	0.17
Case4	0.04	0.23	0.60	0.13
Simulation4	0.15	0.14	0.58	0.13

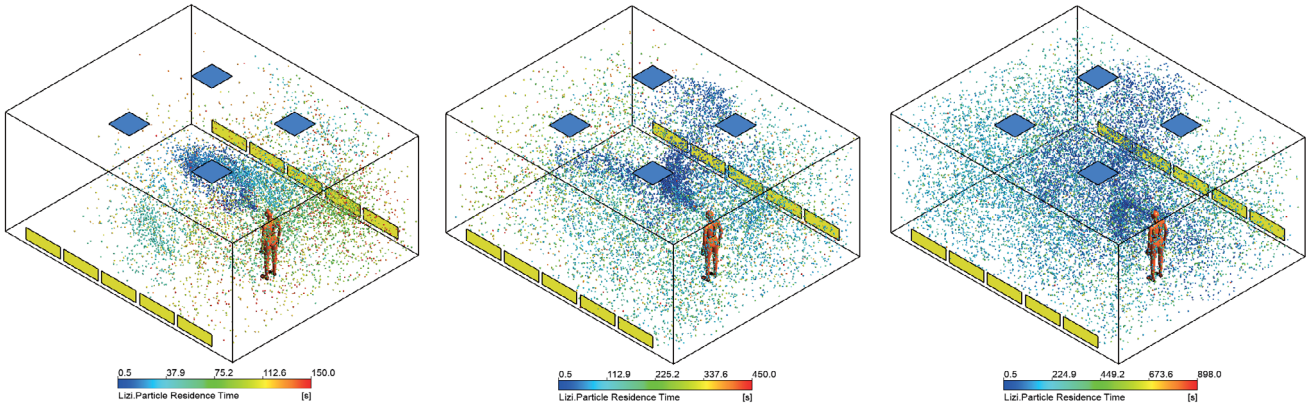

Fig. 8 Aerosols distribution in Case 6 (time = 150 s, 450 s, 900 s)

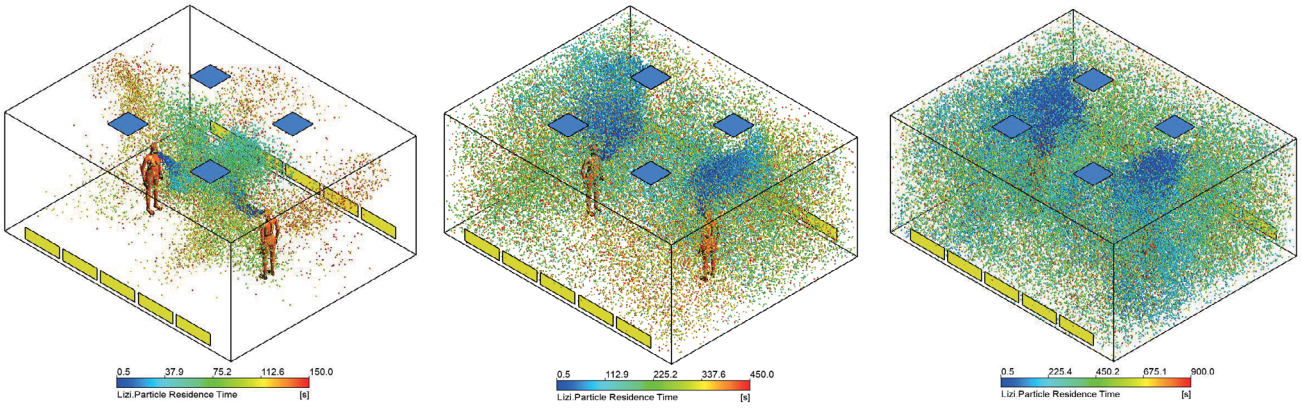

Fig. 9 Aerosols distribution in Case 13 (time = 150 s, 450 s, 900 s)

height of the horizontal section; u_g is the velocity of the air supply; u_i is the initial speed of the particle; T_g is the temperature of the supply air and T_i is the initial temperature of the particle.

For the correlation above:

$$0.25 \le \frac{x}{W}, \frac{y}{L} \le 0.75, 0.27 \le \frac{z}{H} \le 0.53, 0.11 \le \frac{u_g}{u_i} \le 0.22,$$

$$0.37 \le \frac{T_g}{T_i} \le 1.11$$

As shown in Figure 10, the deviations between the calculated values of the regression correlation formula and the numerical simulation results are less than 20%, verifying the reasonable practicability of the correlation formula.

4.4 Comparison of single and multiple people models of bacterial production

Two planes are selected, and six fixed points are chosen for each plane. The concentration of each point is calculated by the particle mass concentration in the 0.03 m^3 spherical area. The air sample collected at each point is 0.03 m^3 (30 L), which was approaching the air sampling volume of the Anderson sampler within one minute. Wang et al. (2018) have also used spheres to calculate particle concentrations.

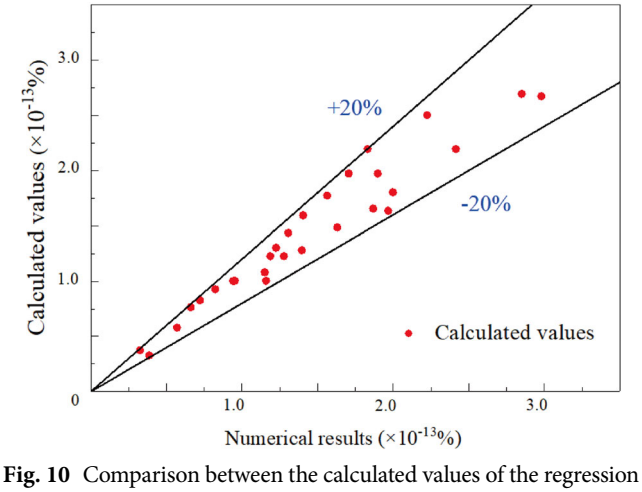

Fig. 10 Comparison between the calculated values of the regression correlation and the numerical simulation results

Figure 11 shows the comparison of particle mass concentration between superposition under single-people cases and multiple-person cases at different heights (z = 0.8 m and z = 1.6 m). Compared the particle mass concentration of two-persons cases and single-person cases. At 450 s, the particle mass concentration at the measuring point 1, point 2, and point 3 at 0.8 m height in the single-person cases (case 1, case 4 and case 7, case 10) was all lower than that at the two-person case (case 13), even several times smaller. However, at point 4, point 5, point 6, the particle mass concentration in the single-person case is mainly greater than that in the multiple-person case. At the height of 1.6 m, the particle mass concentration of the two-person case (case 15) at six measuring points at 900 s showed no obvious pattern compared with that of the single-person cases (case 3, case 6, case 9, case 12). It suggests that the multiple-person -person cases are not a superposition of the data of the one-person cases. One cause may be that the particle distribution is entirely affected by the airflow field and temperature gradient, and some minor changes will cause the large-scale movement of particles. Under such uncontrollable factors, the multiple modes of the single-person model of bacteria production cannot be used in the multi-person model of bacteria production.

5 Conclusion

In this study, the RNG k-ε turbulence model coupled with the Lagrange method was used to conduct CFD simulation on the diffusion and distribution of human exhaled particles in the ventilation room.

The simulation results and experimental data were tallied preferably. According to the particle mass concentration of 18 measuring points at two horizontal heights, 20 cases

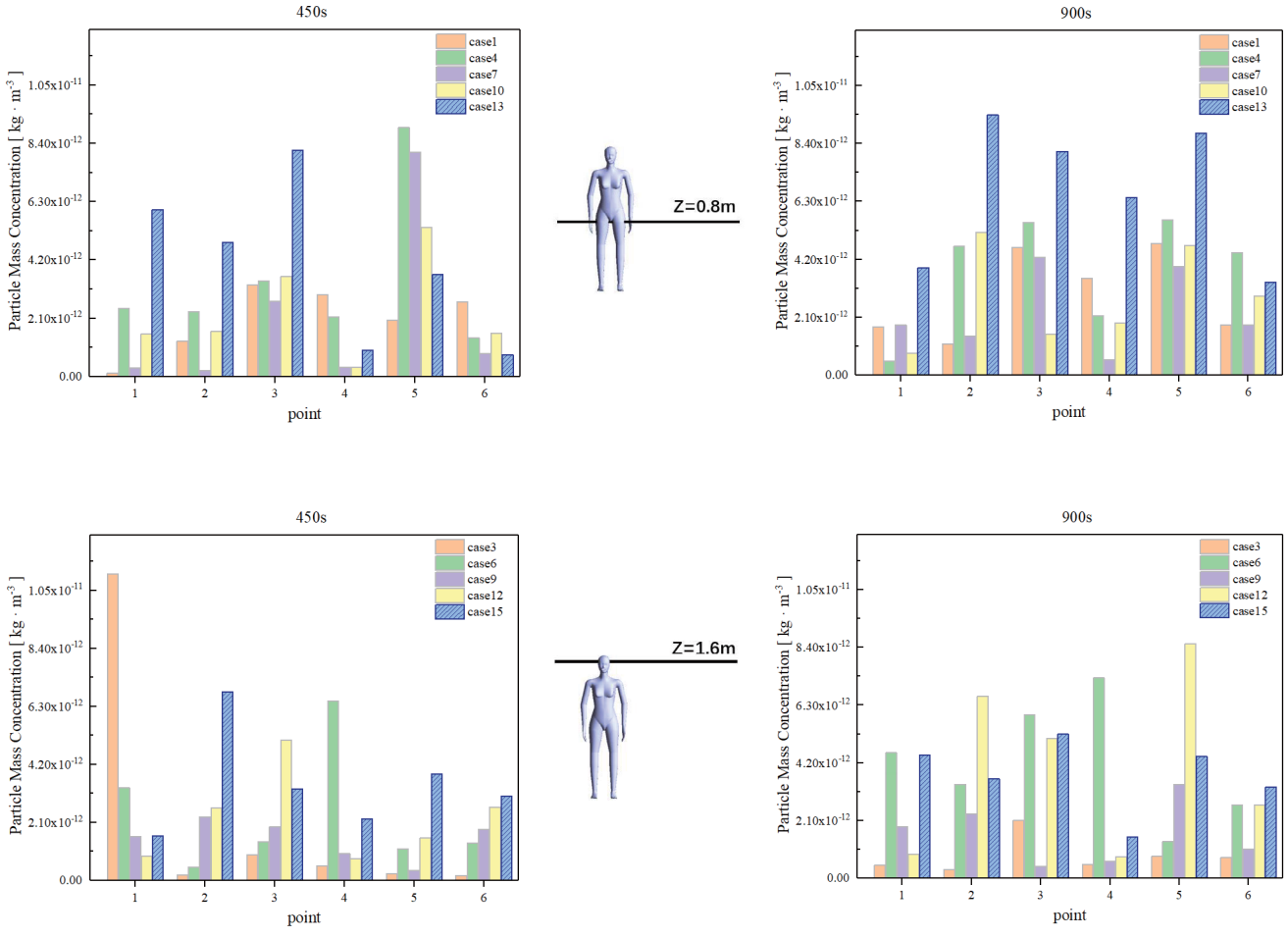

Fig. 11 Comparison of particle mass concentration between superposition under single-people cases and two-people cases at different heights (z = 0.8 m and z = 1.6 m)

with different air supply velocities, air supply temperatures, personnel stations and numbers of personnel were studied. The distributions of human exhaled aerosol in the ventilation room were analyzed and discussed.

(1) The distribution of exhaled aerosol is directly affected by the temperature and air velocity. The aerosol diffuses slowly under the same air supply mode, and it takes a long time to spread throughout the whole ventilation room when the air supply speed at a low speed. However, the larger the air supply velocity, the faster the diffusion of the exhaled aerosol in the ventilation chamber. Therefore, it is not the higher the air supply speed is, the more effective it is to remove indoor particles.

(2) Under different personnel positions and air supply velocities, the aerosol exhaled by the human body will have different diffusion directions at the beginning. When the simulation time is long enough, the particles will always spread to the whole room. On that basis, numerical regression was carried out on the simulated data, and the single-person model of the bacteria production model was obtained. The model can be used to predict the distribution of indoor aerosol under different air supply modes.

(3) The multi-person model of bacteria production is not a superposition of the single-person model of bacteria production. Under the same air supply speed and temperature conditions, when there are many people in the ventilation room, the particle mass concentration at a specific position in the room is not a multiple of the particle mass concentration at a certain position in the single-person model. The reason is related to the complex airflow field and temperature gradient.

In general, both CFD models and real experiments results were combined in the study, and it was verified by the real measurement under similar airflow conditions. A prediction model was established according to the relationship between indoor aerosol pollution level and environmental parameters, which provide purpose guidance for the control of indoor environmental pollution and a valuable scientific basis for the location of air purifiers or the design of a healthy indoor environment. However, the main conclusions obtained from the numerical simulation have not been confirmed by related

experiments. Further research on measuring aerosols in a more realistic situation, such as living room or office with many people, should be carried out.

Acknowledgements

This work was supported by the National Key R&D Program of China (No. 2019YFC1520700), the National Natural Science Foundation of China (No. 41977368), the National Science and Technology Ministry of China (No. 2017YFC0702800), Opening Funds of State Key Laboratory of Building Safety and Built Environment National Engineering Research Center of Building Technology (No. BSBE2017-08).

References

Bourouiba L, Dehandschoewercker E, Bush JWM (2014). Violent expiratory events: On coughing and sneezing. *Journal of Fluid Mechanics*, 745: 537–563.

Chang TJ, Hu TS (2008). Transport mechanisms of airborne particulate matters in partitioned indoor environment. *Building and Environment*, 43: 886–895.

Chen C, Zhao B (2010). Some questions on dispersion of human exhaled droplets in ventilation room: answers from numerical investigation. *Indoor Air*, 20: 95–111.

Chen C, Yao M, Luo X, et al. (2020). Outdoor-to-indoor transport of ultrafine particles: Measurement and model development of infiltration factor. *Environmental Pollution*, 267: 115402.

Chow TT, Yang XY (2003). Performance of ventilation system in a non-standard operating room. *Building and Environment*, 38: 1401–1411.

Chow TT, Lin Z, Bai W (2006). The integrated effect of medical lamp position and diffuser discharge velocity on ultra-clean ventilation performance in an operating theatre. *Indoor and Built Environment*, 15: 315–331.

Chow TT, Wang J (2012). Dynamic simulation on impact of surgeon bending movement on bacteria-carrying particles distribution in operating theatre. *Building and Environment*, 57: 68–80.

Dong S, Liu Y, Zhang N, et al. (2017). Theoretical study of thermophoretic impulsive force exerted on a particle in fluid. *Journal of Molecular Liquids*, 241: 99–101.

Elghobashi S (1991). Particle-laden turbulent flows: direct simulation and closure models. *Applied Scientific Research*, 48: 301–314.

Ge X-Y, Pu Y, Liao C-H, et al. (2020). Evaluation of the exposure risk of SARS-CoV-2 in different hospital environment. *Sustainable Cities and Society*, 61: 102413.

Guo K, Qian H, Zhao D, et al. (2020). Indoor exposure levels of bacteria and fungi in residences, schools, and offices in China: A systematic review. *Indoor Air*, 30: 1147–1165.

He Q, Niu J, Gao N, et al. (2011). CFD study of exhaled droplet transmission between occupants under different ventilation strategies in a typical office room. *Building and Environment*, 46: 397–408.

Hinds WC (1999). Aerosol Technology: Properties, Behavior, and Measurement of Airborne Particles. New York: John Wiley & Sons.

Jo WK, Seo YJ (2005). Indoor and outdoor bioaerosol levels at recreation facilities, elementary schools, and homes. *Chemosphere*, 61: 1570–1579.

Jurelionis A, Gagytė L, Prasauskas T, et al. (2015). The impact of the air distribution method in ventilated rooms on the aerosol particle dispersion and removal: The experimental approach. *Energy and Buildings*, 86: 305–313.

Kalogerakis N, Paschali D, Lekaditis V, et al. (2005). Indoor air quality—Bioaerosol measurements in domestic and office premises. *Journal of Aerosol Science*, 36: 751–761.

Kang Z, Zhang Y, Fan H, et al. (2015). Numerical simulation of coughed droplets in the air-conditioning room. *Procedia Engineering*, 121: 114–121.

Kim J-G, Kim A-H, Kim J-S (2014). Assessment of bioaerosols in public restrooms. *Korean Journal of Environmental Health Sciences*, 40: 304–312.

Lednicky JA, Lauzardo M, Fan ZH, et al. (2020). Viable SARS-CoV-2 in the air of a hospital room with COVID-19 patients. International Journal of Infectious Diseases, 100: 476–482.

Lee KW, Liu BYH (1982). Theoretical study of aerosol filtration by fibrous filters. *Aerosol Science and Technology*, 1: 147–161.

Lee BU, Hong IG, Lee DH, et al. (2012). Bacterial bioaerosol concentrations in public restroom environments. *Aerosol and Air Quality Research*, 12: 251–255.

Lindsley WG, Noti JD, Blachere FM, et al. (2015). Viable influenza A virus in airborne particles from human coughs. *Journal of Occupational and Environmental Hygiene*, 12: 107–113.

Lis DO, Pastuszka JS (1997). Bacterial and fungal aerosol in homes without and with mold problem, in Upper Silesia, Poland. Preliminary results. *Journal of Aerosol Science*, 28: S665–S666.

Liu W, Liu D, Gao N (2017). CFD study on gaseous pollutant transmission characteristics under different ventilation strategies in a typical chemical laboratory. *Building and Environment*, 126: 238–251.

Morawska L, Johnson GR, Ristovski ZD, et al. (2009). Size distribution and sites of origin of droplets expelled from the human respiratory tract during expiratory activities. *Journal of Aerosol Science*, 40: 256–269.

Patankar SV, Spalding DB (1967). A finite-difference procedure for solving the equations of the two-dimensional boundary layer. *International Journal of Heat and Mass Transfer*, 10: 1389–1411.

Romano F, Marocco L, Gustén J, et al. (2015). Numerical and experimental analysis of airborne particles control in an operating theater. *Building and Environment*, 89: 369–379.

Sadrizadeh S, Tammelin A, Ekolind P, et al. (2014). Influence of staff number and internal constellation on surgical site infection in an operating room. *Particuology*, 13: 42–51.

Sassi HP, Reynolds KA, Pepper IL, et al. (2018). Evaluation of hospital-grade disinfectants on viral deposition on surfaces after toilet flushing. *American Journal of Infection Control*, 46: 507–511.

Srebric J, Vukovic V, He G, et al. (2008). CFD boundary conditions for contaminant dispersion, heat transfer and airflow simulations around human occupants in indoor environments. *Building and Environment*, 43: 294–303.

Wang C, Holmberg S, Sadrizadeh S (2018). Numerical study of temperature-controlled airflow in comparison with turbulent mixing and laminar airflow for operating room ventilation. *Building and Environment*, 144: 45–56.

Wang C, Holmberg S, Sadrizadeh S (2021). Impact of door opening on the risk of surgical site infections in an operating room with mixing ventilation. *Indoor and Built Environment*, 30: 166–179.

Wu F, Zhao S, Yu B, et al. (2020). A new coronavirus associated with human respiratory disease in China. Nature, 579: 265–269.

Xie X, Li Y, Chwang ATY, et al. (2007). How far droplets can move in indoor environments—Revisiting the Wells evaporation-falling curve. *Indoor Air*, 17: 211–225.

Yan Y, Li X, Shang Y, et al. (2017). Evaluation of airborne disease infection risks in an airliner cabin using the Lagrangian-based Wells-Riley approach. *Building and Environment*, 121: 79–92.

Yao M, Zhang L, Ma J, et al. (2020). On airborne transmission and control of SARS-Cov-2. *Science of the Total Environment*, 731: 139178.

Zhang Z, Chen Q (2009). Prediction of particle deposition onto indoor surfaces by CFD with a modified Lagrangian method. *Atmospheric Environment*, 43: 319–328.

Zhang Y, Feng G, Kang Z, et al. (2017). Numerical simulation of coughed droplets in conference room. *Procedia Engineering*, 205: 302–308.

Zhao B, Yang C, Yang X, et al. (2008). Particle dispersion and deposition in ventilated rooms: Testing and evaluation of different Eulerian and Lagrangian models. *Building and Environment*, 43: 388–397.

Zukowska D, Melikov A, Popiolek Z (2012). Impact of personal factors and furniture arrangement on the thermal plume above a sitting occupant. *Building and Environment*, 49: 104–116.